Title

Human intestinal tissue-resident memory CD8+ T cells comprise transcriptionally and functionally distinct subsets

Authors (full names and institutions)

Michael E.B. FitzPatrick[1]*, Nicholas M. Provine[1]*, Lucy C. Garner[1]*, Kate Powell[2], Ali Amini[1], Sophie Irwin[1], Helen Ferry[1], Tim Ambrose[1,3], Peter Friend[3], Georgios Vrakas[3], Srikanth Reddy[3], Elizabeth Soilleux[4], Paul Klenerman[1,2,5†], Philip J. Allan[1,3,5]

*MF, NP, and LG contributed equally to this paper

[†]Corresponding author

1 Translational Gastroenterology Unit, Nuffield Department of Medicine, University of Oxford, Oxford, UK

2 Peter Medawar Building for Pathogen Research, University of Oxford, UK

3 Oxford Transplant Centre, Oxford University Hospitals NHS Foundation Trust, Churchill Hospital, Oxford, UK

4 Division of Cellular and Molecular Pathology, Addenbrooke's Hospital, Cambridge, UK

5 NIHR Biomedical Research Centre, John Radcliffe Hospital, Oxford, UK

Summary

Heterogeneity within human tissue-resident memory T (T_{RM}) cells is poorly understood. We show that transcriptionally, phenotypically, and functionally distinct CD4+ and CD8+ T_{RM} subsets exist in the human intestine, and that β2-integrin expression identifies a distinct population of CD8+ T_{RM} cells.

Abstract

Tissue-resident memory T (T_{RM}) cells provide key adaptive immune responses in infection, cancer, and autoimmunity. However transcriptional heterogeneity of human intestinal T_{RM} cells remains undefined, and definitive markers of CD103- T_{RM} cells are lacking. Here, we investigated transcriptional and functional heterogeneity of human T_{RM} cells through the study of donor-derived intestinal T_{RM} cells from intestinal transplant recipients. Single-cell transcriptional profiling identified four conventional T_{RM} populations, with two distinct transcriptional states of CD8+ T_{RM} cells, delineated by *ITGAE* and *ITGB2* expression. We defined a transcriptional signature discriminating the two CD8+ populations, including differential expression of key residency-associated genes and cytotoxic molecules. Flow cytometry of recipient-derived cells infiltrating the graft and intestinal lymphocytes from healthy gut confirmed the two CD8+ T_{RM} phenotypes, with β2-integrin acting as a CD103- CD8+ T_{RM} marker. CD103+ CD8+ T_{RM} cells produced IL-2, and demonstrated greater polyfunctional cytokine production, while β2-integrin+ CD69+ CD103- T_{RM} cells had higher granzyme expression. Phenotypic and functional analysis of intestinal CD4+ T cells identified many parallels, including a distinct β2-integrin+ population. Together, these results describe the transcriptional,

phenotypic, and functional heterogeneity of human intestinal T_{RM} cells, and suggest a role for β2-integrin in T_{RM} development.

Introduction

Tissue-resident memory T (T_{RM}) cells are a subset of long-lived T cells that reside in tissue and do not recirculate (Mackay and Kallies, 2017; Szabo et al., 2019). T_{RM} populations provide rapid, *in situ* adaptive protection against a wide spectrum of pathogens (Gebhardt et al., 2011; Schenkel et al., 2014). T_{RM} cells also have key roles in cancer immune surveillance (Park et al., 2019), and are implicated in autoimmunity, including inflammatory bowel disease (IBD) and coeliac disease (Zundler et al., 2019; Mayassi et al., 2019). CD8+ T_{RM} cells have potent cytotoxic functions and produce pro-inflammatory cytokines to trigger innate and adaptive immune responses (Ariotti et al., 2014).

Murine work has advanced our understanding of T_{RM} cells substantially, however T_{RM} phenotype, transcriptional profiles, and genetic regulation differ between mice and humans (Oja et al., 2017; Hombrink et al., 2016; Kumar et al., 2017). Until recently, human studies of T_{RM} biology were hampered by the inability to prove long-lived tissue residency, with surface molecules CD69 and CD103 (αE integrin) used as surrogate T_{RM} markers. These were used to identify the putative transcriptional signature of human T_{RM} cells, with CD69 hypothesised as the key residency marker (Kumar et al., 2017). However, this gene signature was derived from bulk populations, so it remains unclear if there are transcriptionally distinct subsets within human T_{RM} cells.

Despite its expression on almost all murine and human T_{RM} cells, the use of CD69 as a residency marker has recently been questioned. CD69 restricts lymphocyte tissue egress via S1P1 inhibition, but is not required for the development of functional T_{RM} cells in mice (Shiow et al., 2006; Walsh et al., 2019). CD69 can be induced via stimulation, and a proportion of CD69+ T cells in tissue are not resident, making CD69 a suboptimal residency marker (Shiow et al., 2006; Sancho et al., 2005; Beura et al., 2018). Therefore, additional phenotypic markers to identify CD103- T_{RM} populations are required.

Recent work has exploited the human model of organ transplantation to study long-lived donor-derived T cells, which are definitive functionally resident T_{RM} cells (Zuber et al., 2016; Bartolomé-Casado et al., 2019; Snyder et al., 2019). Studies using this approach have demonstrated persistence of clonally-identical intestinal CD8+ T_{RM} cells for up to 1 year in the small intestine (SI) (Bartolomé-Casado et al., 2019), and of donor-derived T cells for 600 days post-transplant (Zuber et al., 2016). This approach was also used to identify putative SI CD8+ T_{RM} cell subsets based on expression of CD103 and KLRG1, with differences in clonality, granzyme expression, and cytokine production (Bartolomé-Casado et al., 2019). However, it remains unclear whether these cell populations represent transcriptionally distinct subsets.

This work sought to examine the heterogeneity within functionally resident donor-derived T cells in intestinal transplantation using flow cytometry and single-cell RNA

sequencing (scRNAseq). We confirmed that SI CD4+ and CD8+ T_{RM} cells can persist for 5 years post-transplant. scRNAseq identified conventional and regulatory CD4+ T_{RM} cell populations, as well as two transcriptionally distinct CD8+ T_{RM} subsets, which differed in expression of *ITGAE* (CD103, αE integrin) and *ITGB2* (CD18, β2-integrin). These two populations differentially expressed putative T_{RM}-associated genes, indicating that the gene signatures derived from bulk RNAseq data may be a synthesis of several transcriptomic profiles. We validated this phenotypic and functional heterogeneity in the healthy intestine, with increased β2-integrin expression and distinctive effector function in CD103- T_{RM} cells. CD69, β2-integrin, and CD103 expression altered with time post-transplant on recipient-derived graft-infiltrating CD8+ T cell populations, consistent with acquisition of T_{RM} status. We conclude that CD69+ CD103- β2-integrin+ CD8+ intestinal T cells are a transcriptionally and functionally distinct T_{RM} population, and suggest that β2-integrin can serve as a proxy surface marker for the CD103- CD8+ T_{RM} population.

Results and discussion

Long-lived conventional CD4+ and CD8+ T cells, but not innate-like populations, persist long-term in the human intestine

To examine the persistence of resident T cells in the small intestine (SI) post-transplant, we used HLA allele congenic cell tracking, a method allowing discrimination of donor- and recipient-derived cells following transplantation using fluorophore-

116 conjugated antibodies to discordant Class I HLA haplotypes (Fig. 1A, Supplemental Fig.
117 1A) (Zuber et al., 2016; Bartolomé-Casado et al., 2019). The presence of SI donor- and
118 recipient-derived T cells *in situ* was confirmed by chip cytometry (Fig. 1B)(Leng et al.,
119 2019).
120
121 Infiltration of recipient-derived T cells into the graft increased over time, with striking
122 heterogeneity (Fig. 1C). Current or previous rejection was associated with higher
123 proportions of recipient-derived T cells in the graft (Fig. 1D), consistent with prior work
124 (Zuber et al., 2016). Conversely, two individuals had persistent donor-derived SI T cell
125 populations at 4 years 7 months (1684 days) and 5 years 1 month (1865 days) post-
126 transplant (Fig. 1E, and data not shown). This extends previous reports of long-lived
127 donor-chimerism in the human intestine (Zuber et al., 2016; Bartolomé-Casado et al.,
128 2019).
129
130 Haematopoietic stem and progenitor cells can persist in the intestinal transplant
131 graft, sometimes leading to long-term chimerism of donor-derived populations in blood
132 (Fu et al., 2019). This could allow persistence of donor-derived T cells in the graft
133 through continuous ingress from blood, rather than via residency (Bartolomé-Casado et
134 al., 2019). Contrasting with the work of Fu *et al.*, flow cytometric analysis of blood
135 collected from transplant recipients at the time of biopsy revealed the percentage of
136 circulating donor origin T cells was extremely low beyond 3 months post-transplant
137 (median 0.042%, 95% CI 0-1.22%; Fig. 1F). This is far below the posited cut-off for
138 macrochimerism of 4% in previous work (Fu et al., 2019), and similar to background

non-specific staining in non-transplant recipients (0.01-0.12%; Supplemental Fig. 1B), suggesting against continuous replacement as a confounding mechanism for sustained donor chimerism. This discrepancy in circulating chimerism between studies may be due to differences in transplant procedure (multi-visceral vs isolated intestinal transplant in this study) and recipient age (paediatric vs adult in this study) (Zuber et al., 2015; Fu et al., 2019).

Conventional CD4+ and CD8+ T cells dominated in the graft post-transplant (Fig. 1G), and demonstrated similar kinetics of recipient-derived replacement with time (Fig. 1H). We also examined the dynamics of unconventional T cell subsets post-transplant, as their residency characteristics in humans are poorly understood (Supplemental Fig. 1C). CD161+Vα7.2+CD8+ T cells (consistent with mucosal-associated invariant T (MAIT) cells), and Vδ2+ γδ T cells (which possess analogous innate-like functions to MAIT cells (Provine et al., 2018; Gutierrez-Arcelus et al., 2019)) were rare in the graft post-transplant, recovering to expected frequencies after 1 year (Fig, 1I) . However, the non-Vδ2 γδ T cell subsets demonstrated different dynamics, with this population present at early timepoints. Unconventional T cell subsets demonstrated similar replacement kinetics (Fig. 1J). It is unclear if the low innate-like T cell frequency post-transplant is due to differences in residency characteristics, or to increased sensitivity to the ischaemic insult of surgery or perioperative conditioning regimes.

We examined CD69 and CD103 expression on donor- and recipient-derived CD4+ and CD8+ T cell populations in the intestinal graft. CD103 expression was restricted to

CD69+ cells, with a greater proportion of CD8+ cells expressing CD103 than CD4+ cells(Fig. 1K), in keeping with prior work (Kumar et al., 2017). Donor-derived T cells showed near-ubiquitous expression of CD69 consistent with a lack of recent migration from blood, and had fewer CD69- cells than recipient-derived populations for both CD8+ (median 0.03% vs 4.17%, $p<0.0001$, Wilcoxon signed rank test) and CD4+ cells (median 0.10% vs 5.65%, $p<0.0001$, Wilcoxon signed rank test) (Fig. 1L). This suggests that CD69- T cells in the SI are not functionally resident in humans, in contrast to recent murine data which showed no functional requirement for CD69 to establish intestinal residency (Walsh et al., 2019). Recipient-derived CD4+ and CD8+ T cell populations showed increasing expression of CD103 with time, consistent with the acquisition of a T_{RM} phenotype, as in prior work (Zuber et al., 2016). We have previously shown higher expression of the C-type lectin-like receptor CD161 on intestinal CD103+ CD8+ T cells (Fergusson et al., 2015); here a greater proportion of donor-derived CD8+ T cells expressed CD161, consistent with an association with residency (Supplemental Fig. 1D,E).

Single-cell RNA sequencing delineates transcriptionally distinct states within CD4+ and CD8+ T_{RM} populations

The persistence of CD103- and CD103+ donor-derived T cells up to five years post-transplant, and the enrichment of CD103+ recipient-derived T cells at later time points, raised the possibility that CD103- and CD103+ T cells represented distinct cell states. To test this hypothesis, we performed droplet-based scRNAseq of sorted donor-derived

185 graft-resident T_{RM} cells from a single subject one year post-transplant (Experiment 1,
186 Fig. 2A). 1,774 cells were captured and sequenced, with 974 cells remaining after
187 filtering (Supplemental Fig. 2A).
188
189 Four transcriptionally distinct clusters were identified (Fig. 2B): conventional CD4+ T
190 cells, regulatory CD4+ T cells expressing *IL2RA* and *FOXP3*, and two clusters of
191 conventional CD8+ T cells (Fig. 2C). The differentially expressed genes (DEGs)
192 between the two populations of donor-derived CD8+ T_{RM} cells (hereafter CD8+
193 population 1 and 2) were analysed (Fig. 2D). Population 1 expressed *ITGAE* (CD103),
194 as well as higher levels of *CD7*, *IL7R* (CD127), *KLRB1* (CD161), and the chemokine
195 receptor *CCR6* (Fig. 2E). IL-7, a stromal-derived homeostatic cytokine which provides
196 survival and proliferative signals to lymphocytes (Raeber et al., 2018), is required for
197 epidermal T_{RM} persistence (Adachi et al., 2019), and *CD127* is highly expressed in SI
198 memory T cells (Thome et al., 2014). The differential expression of IL7R suggests
199 differences in the mechanisms, or nature, of T_{RM} persistence between the two
200 populations (Raeber et al., 2018).
201
202 Conversely, CD8+ population 2 expressed low levels of *ITGAE*, but high levels of
203 *KLRG1*, as well as cytotoxic granzyme molecules and class II MHC molecules (Fig.
204 2D,E). Surface KLRG1 expression can delineate two putative SI CD103- CD8+ T cell
205 subsets with similar residency characteristics (Bartolomé-Casado et al., 2019).
206 However, population 2 did not sub-cluster further based on *KLRG1* gene expression,
207 suggesting that these are not transcriptionally distinct states. Of particular interest, the

integrin *ITGB2* (β2-integrin/CD18), was highly expressed by the CD103- CD8+ population 2. β2-integrin can form heterodimers with four α-integrins (Fagerholm et al., 2019), only one of which, *ITGAL* (CD11a), was detected in the dataset. *ITGAL* was highly expressed on the CD103- CD8+ population 2 (Supplemental Fig. 2B,C).

CD8+ CD103+ and CD103-ITGB2hi T_{RM} subsets differ in expression of putative residency-associated genes

Transcriptional signatures associated with human tissue residency have been defined, most thoroughly by bulk RNA sequencing of CD69- and CD69+ T cells from multiple tissues (Kumar et al., 2017). This T_{RM} gene set was explored in the two CD8+ T cell populations. The genes downregulated in CD69+ T cells were either not detected, or found at low levels in both clusters (Supplemental Fig. 2D,E). However, several T_{RM}-associated genes upregulated in CD69+ T cells were differentially expressed between the two clusters, with population 1 expressing higher levels of *ITGAE* and *ITGA1* (in agreement with work on renal T_{RM} cells (de Leur et al., 2019)), and population 2 expressing higher levels of *CRTAM* (Fig. 2F, Supplemental Fig. 2F). In addition, *ZNF683* (Hobit), a transcriptional regulator of residency in mice (Mackay et al., 2016), was more highly expressed in population 1. These data indicate that previously identified T_{RM} gene signatures may represent an amalgamation of several distinct T_{RM} transcriptional states.

To confirm the presence of transcriptionally distinct CD8+ T_{RM} states, a second

scRNAseq experiment was performed on samples from two further transplant recipients (Experiment 2, Fig. 2A). Donor-derived CD103- and CD103+ CD8+ T cells were index-sorted before plate-based scRNAseq using the Smart-Seq2 protocol (Picelli et al., 2013). 267 cells were sorted and sequenced, with 196 cells remaining post-filtering (Supplemental Fig. 2G-I). Three clusters were identified, with cluster 1 predominantly formed of CD103- T cells, and the transcriptionally similar clusters 2 and 3 formed of CD103+ T cells (Fig. 2G). Clusters 2 and 3 (CD103+) expressed higher levels of *ITGAE*, *CD7*, and *IL7R*, while cluster 1 (CD103-) expressed higher levels of *GZMK*, *GZMH*, class II HLA molecules, and *ITGB2* (Fig. 2H). *ITGAL*, was also detected in cluster 1 (Supplemental Fig. 2J).

Differential expression analysis between cluster 1 and clusters 2 and 3 combined revealed similar transcriptional differences to those in Experiment 1 (Fig. 2I, Supplemental Table 2). Comparison of DEGs in the two experiments identified a core set of 30 genes that distinguished the two populations (Fig. 2I,J).

Putative T_{RM} cell subsets in the context of lung transplantation have been described, however these did not align with CD103 expression (Snyder et al., 2019), in contrast to our work. The transcriptional signatures of the clusters were also different in our work, with the exception of *ZNF683*, which was also associated with one lung T_{RM} subset. These differences may reflect tissue-specific gene signatures in T_{RM} cells, differences in CD4+ and CD8+ T_{RM} cells, which co-clustered in the previous study of lung T_{RM} cells, or may be an effect of increased cell number in this study, allowing greater power to detect

254 transcriptionally distinct sub-clusters.

255

256 ***CD103+ and CD103- CD8+ T cells display distinct phenotypes in the healthy***
257 ***intestine***

258

259 The presence of CD103- and CD103+ donor-derived CD8+ T cells in the
260 transplanted SI mucosa was confirmed using chip cytometry (Fig. 3A). Flow cytometry
261 of donor-derived T cells demonstrated differences in expression of CD161, β2 integrin,
262 and granzyme K between CD103- and CD103+ CD8+ T cells, consistent with
263 scRNAseq data (Supplementary Fig. 3A).

264

265 To validate the phenotypic differences between the two putative SI CD8+ T_{RM}
266 subsets outside the transplant setting, we performed flow cytometry of SI T cells from
267 healthy donors. CD8+ SI T cells expressing both CD69 and CD103 predominated,
268 representing 88.9% (81.7-96.0%) of CD8+ T cells, with no difference seen between SI
269 location (Supplementary Fig. 3B).

270

271 CD103+ CD8+ T cells expressed higher levels of CD161 and CD127 (IL7R)
272 compared with the CD69- or CD69+CD103- cells, consistent with the transcriptomic
273 data (Fig. 3B,C). CD7 expression was higher on all CD69+ T cells, with no difference
274 seen between CD69+CD103- and CD69+CD103+ populations. In contrast,
275 CD69+CD103- CD8+ T cells expressed higher levels of β2-integrin, granzyme K, and
276 KLRG1 than either CD69- cells or CD69+CD103+ cells.

Ki-67 expression formed a gradient between the three populations, with higher expression in the CD69- population, and a trend towards increased Ki67 expression in CD69+CD103- CD8+ T cells compared to CD103+ CD8+ T cells (mean 14.88% vs 5.72%, 1-way ANOVA and Tukey's multiple comparisons test, P=0.067). This is consistent with prior work indicating that T_{RM} cell persistence is due to longevity rather than *in situ* proliferation (Thome et al., 2014).

Graft-infiltrating, recipient-derived T cells take on a T_{RM} phenotype over time, with CD103+ and CD103- CD8+ T cells displaying distinct phenotypes

To explore the dynamics of T_{RM} phenotype acquisition, we examined graft-infiltrating, recipient-derived T cells. In the early post-transplant period, 52.7% of infiltrating CD8+ T cells lacked CD69 expression, with acquisition of the CD69+ CD103+ T_{RM} phenotype over time (Fig. 3D). At later times post-transplant, CD103- and CD103+ populations clearly differed in phenotype, consistent with the two subsets seen in healthy SI. CD161 expression was higher on CD103+ CD8+ T cells than CD69+CD103- T cells, and granzyme K expression was higher on CD69+CD103- CD8+ T cells (Fig. 3E-H). A similar gradient of Ki-67 expression between the populations was seen (Fig. 3F). In addition, graft-infiltrating CD69+CD103- CD8+ T cells demonstrated higher expression of β2 integrin than either CD69- or CD103+ populations (Fig. 3I). β2 integrin expression is constitutively high on circulating T cells (Fig. 3J), as LFA-1 is involved in tissue entry via ICAM-1 (Fagerholm et al., 2019). These data suggest that β2 integrin

surface expression is reduced on recent tissue immigrants, before subsequent up regulation on CD69+CD103- T_{RM} cells, but not on CD103+ T_{RM} cells. Recipient-derived CD8+ T cells infiltrating the graft in the early post-transplant period displayed less clear distinctions between populations, although the small number of samples precluded further analysis.

CD103+ CD8+ intestinal T cells demonstrate greater capacity for cytokine production

To assess cytokine production capacity of these subsets, SI T cells from healthy controls were stimulated for four hours with PMA+ionomycin, before intracellular flow cytometry for TNFα, IFNγ, IL-2, CCL4, IL-17A, and IL-10. 77% of CD103+ CD8+ T cells produced at least one cytokine, a greater proportion than CD69+CD103- CD8+ T cells (47.7% cytokine positive, P<0.0001), and CD69- CD8+ T cells (37% cytokine positive, P<0.0001) (Fig. 4A-F). CD69+ populations produced more TNFα and IFNγ than CD69- cells, irrespective of CD103 expression (Fig. 4A,B). While scRNAseq data indicated increased *CCL4* transcripts in CD69+CD103- CD8+ T cells, CCL4 production following stimulation was not different between the two CD69+ populations (Fig. 4C).

CD103+ CD8+ T cells expressed more IL-2 than either CD69+CD103- or CD69- populations (Fig. 4D). Hepatic CD103+ CD8+ T_{RM} cells also produce increased IL-2 (Pallett et al., 2017). Autocrine IL-2 production is critical to secondary proliferative responses and IFNγ production in CD8+ T cells (Feau et al., 2011), and may be of

particular relevance to intra-epithelial lymphocyte populations, where the infrequent CD4+ T cells may provide suboptimal help (Zimmerli et al., 2005).

There was a spectrum of functionality between the three populations, with CD69- CD8+ T cells predominantly non- or mono-functional, CD103+ CD8+ T cells predominantly polyfunctional, and CD69+CD103- CD8+ T cells showing intermediate functionality (Fig. 4E,F), consistent with a prior report (Bartolomé-Casado et al., 2019). Quadruple functional cells were more common in the CD103+ population than in the CD69+CD103- population (21.76% vs 10.32%, P<0.0001), and were near-absent in the CD69- population (0.38%). These results demonstrate that the transcriptionally distinct CD103- and CD103+ CD8+ T_{RM} populations differ functionally and phenotypically, with CD103+ CD8+ populations more polyfunctional, and producing IL-2.

CD103+ and CD103- CD4+ T cells display analogous phenotypic and functional differences to their CD8+ counterparts

Despite not forming transcriptionally distinct clusters by scRNAseq, CD4+ SI T cells differed in their phenotype, dependent on CD69 and CD103 expression. CD69- populations expressed lower levels of CD161 and CD127, while CD69+CD103- CD4+ T cells had higher expression of β2-integrin than either CD69- or CD103+ populations, analogous to their CD8+ counterparts (Fig. 5A). Recipient-derived, graft-infiltrating CD69+CD103- CD4+ T cells also displayed higher expression of β2-integrin than CD103+ counterparts (MFI 51,753 vs 30,959, P<0.0001; Fig. 5B).

A donor-derived regulatory CD4+ FOXP3+ population was detected in the scRNAseq data (Fig. 2C), and donor-derived CD25+CD127- CD4+ T cells were detected by flow cytometry in some subjects, consistent with potential long-term residency of SI CD4+ regulatory T cells (Supplementary Fig. 3C). Low cell number of this population precluded further analysis.

CD69+ CD4+ SI T cells showed higher production of multiple cytokines upon short-term stimulation compared with CD69- T cells (Fig. 5C-I). In particular, IL-17A production was almost exclusively restricted to CD69+ T cells (Fig. 5C). CD103+ CD4+ T cells demonstrated higher production of TNFα, CCL4, IL-17A, and IL-10 than CD69+ CD103- counterparts. There was a similar gradient of functionality between the three CD4+ populations, with CD103+ cells showed greatest polyfunctional cytokine production (Fig. 5I), as seen in CD8+ T cells. In summary, CD4+ SI T cell populations demonstrated analogous differences in phenotype and functionality to their CD8+ counterparts.

Discussion

This study has identified two transcriptionally distinct states of functionally-resident *bona fide* human intestinal CD8+ T_{RM} cells, which differ in phenotype and cytokine production. This was demonstrated using the rigorous approach of identifying donor-derived populations in the intestinal graft post-transplant, which confirms functional

tissue residency. These data were replicated both within graft-infiltrating T cell populations establishing residency *de novo*, and in the healthy gut. The CD8+ T_{RM} subsets differ in the expression of several genes previously associated with the human T_{RM} signature, which suggests that these signatures, derived from bulk RNAseq data, may represent an amalgam of transcriptionally distinct T_{RM} subsets (Kumar et al., 2017).

The two identified CD8+ T_{RM} populations differ in IL7R (CD127) expression, and in IL-2 production, which may indicate differing persistence and proliferation properties, as well as in the expression of chemokine receptors and integrins, indicating potential differences in tissue homing and retention. Of particular interest, β2-integrin is more highly expressed on CD69+CD103- T_{RM} cells, a population which remains difficult to positively distinguish from recent immigrants from the circulation. β2-integrin could, in addition to CD69, represent an important positive marker to identify this population.

β2-integrin forms part of the heterodimer LFA-1, which facilitates firm adhesion on blood vessel endothelium via ICAM-1, a critical stage in lymphocyte trafficking (Fagerholm et al., 2019). β2-integrin also regulates the immunological synapse providing a co-stimulatory signal, both in the interaction with antigen-presenting cells, and with infected target cells (Liu et al., 2009). LFA-1 is up-regulated on liver-resident T cells and facilitates their patrolling of hepatic sinusoids, indicating a role for LFA-1 in T_{RM} motility and tissue surveillance (McNamara et al., 2017). Intriguingly, the interaction of LFA-1 with ICAM-1 reduces cellular responses to TGFβ, a key cytokine in T_{RM} development (Verma et al., 2012), while TGFβ can inhibit LFA-1 expression and

392 function (Boutet et al., 2016). This suggests a role for β2-integrin in the development of
393 CD103- CD8+ T_{RM} cells, which may be TGFβ-independent, as in mice (Bergsbaken and
394 Bevan, 2015).
395
396 The *ITGB2* locus is a differentially methylated region in the blood and mucosa in
397 IBD, and mucosal gene expression is associated with disease activity (Kennedy et al.,
398 2016; Harris et al., 2014; Román et al., 2013). We hypothesize that this association with
399 IBD, in which T_{RM} cells play a key role (Zundler et al., 2019), could be mediated via
400 altered β2-integrin expression and its effects on T_{RM} cells, or suggest a pathogenic role
401 for one of the two T_{RM} subsets.
402
403 Single-cell transcriptional heterogeneity has previously been examined in lung T_{RM}
404 cells, with two potential subsets identified, characterised by predominantly different
405 gene signatures to those in our study (Snyder et al., 2019). However, their putative
406 subsets contained both CD4+ and CD8+ cells co-clustering, which separated clearly in
407 our study. T_{RM} cell phenotype and behaviour in lung and intestine differ substantially,
408 and this finding may be driven by such tissue-specific differences, or be an effect of the
409 higher cell number in our study (Thome et al., 2014). It remains unclear if analogous
410 subsets to the intestinal populations described in this study exist in other tissues,
411 whether such subsets differ in residency characteristics and functional capacity, and
412 whether they play distinct roles in human health and disease.
413
414 In conclusion, we have used the human model of intestinal transplantation to study

single-cell heterogeneity in the donor-derived *bona fide* T_{RM} intestinal T cells. We found that CD8+ T_{RM} cells form two transcriptionally, phenotypically, and functionally distinct subsets, with parallel findings in CD4+ T cells. In particular, we report the association between β2-integrin and CD69+CD103- intestinal T_{RM} cells, which may prove not only a useful marker for this population, but could also have a role in T_{RM} development and function.

Materials and methods

Human biological material

Intestinal transplant recipients were identified via the Oxford University Hospitals NHS Foundation Trust (OUHFT) transplantation service (Oxford, United Kingdom). Healthy control study subjects were identified via the OUHFT endoscopy service at the time of routine endoscopy. Peripheral blood and intestinal biopsies were taken at the time of endoscopy under the study framework and consent of the Oxford Gastrointestinal Illnesses Biobank (REC Ref: 16/YH/0247). Patient and sample characteristics are described in Supplementary Table 1.

Small intestinal biopsies were collected at the time of endoscopy and transported in R10 (RPMI-1640 [Lonza] + 10% FCS [Sigma-Aldrich] + 1% penicillin/streptomycin [Sigma-Aldrich]), before cryopreservation in freezing medium (10% DMSO [Sigma-Aldrich], 90% FCS [Sigma-Aldrich]). This method preserves immune cell viability, surface marker expression, and function (Konnikova et al., 2018). When required, samples were rapidly thawed in a 37^{o}C water bath, washed in 20ml R10 before tissue dissociation.

Duodenal samples were incubated in R10 media with 1mg/ml Collagenase D (Roche) and 100µg/ml DNase (Thermo Fisher Scientific) for one hour in a shaking incubator at 37^{o}C. Biopsies were then dissociated by vigorous agitation using a GentleMACS Dissociator (Miltenyi Biotec), then strained through a 70µm filter. Cells were washed with R10 media. For samples undergoing *ex vivo* stimulation or cell sorting, the mononuclear cells were isolated on a discontinuous 70% and 35% Percoll

gradient (GE Healthcare) by centrifugation at 700g for 20 minutes without brake. Mononuclear cells were collected from the interface and washed in R10.

For multiplex fluorescence chip cytometry, single intestinal biopsies were embedded in OCT cryo-embedding matrix (Thermo Fisher Scientific) then frozen in isopentane (Sigma-Aldrich) suspended over liquid nitrogen, and stored at -80^{o}C until use.

Peripheral blood mononuclear cells (PBMCs) were isolated from subject blood samples by density gradient centrifugation. In brief, blood was diluted 1:1 with PBS, then layered onto Lymphoprep (Axis-Shield), and centrifuged at 973g for 30 minutes without brake. The mononuclear layer was collected and washed with R10. Any remaining red blood cells were lysed with ACK (Ammonium-Chloride-Potassium) solution for 2-3 minutes, and washed again in R10, before cryopreservation in freezing medium as above.

***Ex vivo* stimulation**

Ex vivo stimulation was performed as previously described (Provine et al., 2018). In brief, purified intestine-derived mononuclear cells were plated at approximately 1x10^{6}/well in a U-bottom 96-well plate. Cell stimulation cocktail containing phorbol 12-myristate 13-acetate (PMA) and ionomycin (Biolegend) was added in accordance with manufacturer's instructions in the presence of brefeldin A and monensin (both Biolegend). Cells were incubated at 37^{o}C, 5% CO_2, for 4 hours.

Flow cytometry and cell sorting

484

485 For surface marker staining, cells were stained in 50µL of FACS buffer (PBS + 1mM
486 EDTA + 0.05% BSA) for 30 minutes at 4°C. Surface antibodies and clones used were:
487 CD3 (OKT3 or UCHT1), Vδ2 (B6), CD4 (OKT4 or SK3), Vα7.2 (3C10), CD38 (HIT2),
488 CD103 (Ber-ACT8), γδTCR (11F2), CD69 (FN50), HLA-A2 (BB7.2), HLA-A3 (GAP.A3),
489 CD8 (SK1 or RPA-T8), CD161 (191B8), nearIR and zombie yellow fixable viability dye
490 (Thermo Fisher Scientific or Biolegend), β2 integrin/CD18 (L130), CD25 (2A3), KLRG1
491 (REA261), CD127 (A019D5), CD7 (M-T701).

492 For intracellular cytokine staining, after surface staining as above, cells were fixed
493 and permeabilised in 100µL Cytofix/Cytoperm solution for 20 minutes at 4°C (BD
494 Biosciences). Cells were then washed twice in Perm/Wash buffer (BD Biosciences).
495 Intracellular staining was performed in 50µl of Perm/Wash buffer (BD Biosciences) for
496 30 minutes at 4°C using the following antibodies and clones: CCL4 (D21-1351), Ki67
497 (B56), TNFα (MAb11, IL-17A (BL168), IFNγ (B27), IL-2 (MQ1-17H12), GzmK
498 (GM26E7), IL-10 (JES3-9D7).

499 After staining, cells were stored at 4°C protected from light until data acquisition.
500 Flow cytometry data were acquired on a BD LSRII flow cytometer (BD BioSciences) or
501 Aurora spectral flow cytometer (Cytek). For fluorescence-activated cell sorting (FACS)
502 samples were surface stained as above, with DAPI (Thermo Fisher Scientific) used as
503 viability dye. FACS was performed on an AriaIII (BD Biosciences; 70µm nozzle).
504 Antibodies were purchased from BioLegend, BD Biosciences, Miltenyi Biotec, or
505 Thermo Fisher Scientific.

506

Flow cytometry data analysis and statistics

Flow cytometry data were analysed using FlowJo version 9.9.5 and version 10.6.1 (FlowJo, LLC). Statistical analyses of flow cytometric data were performed using Prism version 8 (Graphpad Software). For phenotypic analysis of rare cell subsets, populations with fewer than 10 cells were excluded.

Chip cytometry

Samples were frozen in OCT (as described above), cryosectioned onto coverslips and placed in cytometer chips (Zellsafe Tissue chips, Zellkraftwerk, GmbH, Deutscher Platz 5c, 04103 Leipzig, Germany). Sections were fixed *in situ* at room temperature for 10 minutes using 4% paraformaldehyde, then washed with 10 mL of PBS. Non-specific binding was blocked by incubating in 5% goat serum (Thermo Fisher Scientific) in PBS for 1 hour at room temperature. Fluorophore-conjugated antibodies (as above, plus pan-cytokeratin (C-11, GeneTex), and Histone-H3 (17H2L9, Thermo Fisher Scientific)) were diluted for staining in PBS. Immunostaining was performed iteratively, with up to three colours applied simultaneously. Fluorophores were then bleached and additional antibodies applied to build up the panel (Hennig et al., 2009). Images were acquired using a Zellscanner One Chip cytometer (Zellkraftwerk) and ZellExplorer software.

10x Genomics library preparation and sequencing

scRNAseq libraries were generated using 10x Genomics Chromium Single Cell V(D)J Reagents Kits (v1 Chemistry) following manufacturer's instructions. Cells were

resuspended in PBS with 0.04% BSA at ~1000 cells/μL and loaded onto a single lane of the Chromium Controller. Captured cell number was 1,774. Library quality and concentration was determined using a TapeStation (Agilent) and Qubit 2.0 Fluorometer (Thermo Fisher Scientific). Libraries were sequenced on an Illumina HiSeq 4000 as per manufacturer's instructions to a mean depth of 63,471 mean reads/cell. Library generation and sequencing were performed at the Oxford Genomics Centre (Wellcome Centre for Human Genetics, University of Oxford).

Smart-Seq2 library preparation and sequencing

Single cells were index-sorted into 96-well plates with one cell per well in 2.3 μl lysis buffer (0.8% (vol/vol) Triton X-100 and 2 U/μL RNase inhibitor). Smart-Seq2 libraries were generated following the published protocol with External RNA Controls Consortium (ERCC) RNA (1:100,000) added prior to sequencing (Picelli et al., 2014). cDNA was pre-amplified by PCR (21 cycles). Libraries were sequenced on an Illumina HiSeq4000 with 75bp paired-end reads. Library generation and sequencing were performed at the Oxford Genomics Centre (Wellcome Centre for Human Genetics, University of Oxford).

Droplet-based (10x Genomics) scRNAseq data analysis

FastQ generation, read alignment, barcode counting and UMI counting were performed using the Cell Ranger pipeline v2.2.0. Downstream processing steps were performed using Seurat v2.3.4 (Butler et al., 2018; Stuart et al., 2019). Briefly, TCR and

553 BCR genes, and genes expressed in fewer than 10 cells, were removed. Cells with <
554 3460 UMIs (local minimum of the UMI distribution to the left of the mode UMI count), <
555 500 genes, and > 10,000 UMIs, > 2500 genes, and/or > 10% mitochondrial reads were
556 removed (Supplementary Fig. 2A). Variable genes were identified using M3Drop
557 (Andrews et al., 2018). Data were log normalised and scaled, with cell-cell variation
558 due to UMI counts, percent mitochondrial reads, and S and G2M cell cycle scores
559 regressed out. The top 10 principal components (PCs) were used as input for graph-
560 based clustering (0.4 resolution), as determined by visual inspection of the scree plot.
561 Clusters were visualised by tSNE. Differential gene expression analysis between
562 clusters was performed using the Wilcoxon Rank Sum test (FindMarkers function with
563 default parameters).
564
565 ***Plate-based (Smart-Seq2) scRNAseq data analysis***
566
567 Reads were trimmed to remove contaminating adapter and oligo-dT primer
568 sequences using Trimmomatic v0.36 (Bolger et al., 2014). Trimmed reads were aligned
569 to the human genome (hg38 assembly) plus added ERCC “spike-in” sequences using
570 STAR v2.5.3a (--outFilterMismatchNoverLmax 0.04 --outFilterType BySJout --
571 outMultimapperOrder Random) (Dobin et al., 2012). Alignments were filtered using
572 Samtools v1.6 (Li et al., 2009) to retain only primary alignments and properly paired
573 reads. Ensembl gene counts were generated using featureCounts v1.6.0 (-C -B -p)
574 (Liao et al., 2014). Poor quality cells that fit one or more of the following criteria were
575 removed from the analysis (Supplementary Fig. 2G-I): small log-library size (< 3 median

absolute deviations (MADs) below the median), low percentage of uniquely mapped reads (< 55%), low gene count (< 3 MADs below the median), high percentage of ERCCs (> 37.5%), or high mitochondrial read fraction (> 6%). Outlier cells with a large library size or high gene count (potential doublets) were also removed. Genes with "undetectable" expression were removed (gene defined as "detectable" if at least 5 read counts in two cells), along with TCR (and BCR) genes. Log normalised expression values were generated using the normalize function from scater v1.10.1 (McCarthy et al., 2017) with cell-specific size factors calculated using scran v1.12.1 (Lun et al., 2016). Feature selection was performed using M3Drop v3.10.4 (FDR < 0.01) (Andrews et al., 2018) and the expression matrix subset to retain only the selected genes. Clustering analysis was performed using SC3 v1.12.0 (Kiselev et al., 2017). Clusters were visualised by UMAP generated using the top 30 PCs (McInnes et al., 2018) (generated using the top 30 principal components). Differential gene expression analysis was performed using DEsingle v1.2.1 (Miao et al., 2018) (FDR < 0.05).

Upon publication, data will be deposited in the NIH GEO database.

Supplemental material:

- Supplemental Figure 1
- Supplemental Figure 2
- Supplemental Figure 3
- Table 1: Subject and sample characteristics
- Table 2: Differentially expressed gene list

Author contribution

MF, NP, LG, PK, and PA conceived and designed the study. Patient identification, consent, and sample collection was performed by MF, TA, PF, GV, SR, and PA. Experiments and analyses were performed by MF, NP, LG, KP, AA, SI, and HF. Cell sorting was performed by HF. MF, NP, and LG created the figures. MF drafted the article. MF, NP, LG, KP, AA, SI, HF, TA, PF, GV, SR, ES, PK, and PA critically revised the article and approved the final version.

Acknowledgments

We thank the Oxford TGU GI illnesses biobank team, and the clinicians and endoscopists at Oxford University Hospitals NHS Foundation Trust, for assistance in patient identification and sample collection. We are grateful to Dr Chris Willberg and Joachim Hagel at the Peter Medawar Building for work establishing the chip cytometry facility. We are grateful to Professor Laura Mackay for her advice in the conception of this project.

We thank the Oxford Genomics Centre at the Wellcome Centre for Human Genetics (funded by Wellcome Trust grant reference 203141/Z/16/Z) for the generation of sequencing data. The research was funded by the Wellcome Trust (WT 109665MA), NIHR Senior Fellowship (PK), and National Institute for Health Research (NIHR) Oxford Biomedical Research Centre (BRC). The authors have no additional financial interests. The views expressed are those of the author(s) and not necessarily those of the NHS, the NIHR or the Department of Health.

Figure 1. **Conventional T cell subsets persist for 5 years post-transplant, and display a characteristic tissue resident memory (T_{RM}) phenotype.**

(A) Representative flow cytometry plot of HLA-A2 expression of T cells from the blood, the recipient native intestinal mucosa, and the intestinal transplant graft, demonstrating identification of donor- and recipient-derived populations by HLA mismatch.

(B) Representative chip cytometry image of intestinal graft mucosa demonstrating presence of donor-derived (HLA-A2+, yellow arrows) and recipient-derived (HLA-A2-, white arrows) CD3+ T cells in the lamina propria. Cytokeratin (grey); CD3 (purple); HLA-A2 (green).

(C) Percentage of recipient-origin CD3+ T cells in intestinal grafts, categorised by time post-transplant (n=37; mean +/- SEM).

(D) Percentage of recipient-origin CD3+ T cells in intestinal grafts, categorised by history of graft rejection. Unfilled circles, no rejection; Black, current rejection; Grey, previous (post) rejection. (n=37; mean +/- SEM).

(E) Flow cytometry plot of HLA-A3 expression of graft-derived T cells in one subject who demonstrated persistent donor chimerism in the intestinal graft 1865 days (5 years and 1 month) post-transplant.

(F) Percentage of donor-origin CD3+ T cells in the blood of intestinal transplant recipients, categorised by time post-transplant (n=14; mean +/- SEM). Dashed line at 4% represents the cut-off for significant macrochimerism from prior studies (Fu et al., 2019; Zuber et al., 2015).

(G) Conventional CD8+ and CD4+ T cell subsets in the small intestinal graft as a proportion of total T cells, categorised by time post-transplant (n=41; mean +/- SEM).

(H) The percentage of recipient-derived T cells infiltrating the intestinal graft within conventional CD8+ and CD4+ T cell subsets, categorised by time post-transplant (n=41; mean +/- SEM).

(I) Unconventional non-Vδ2+ γδ T cell, Vδ2+ γδ T cell, and Vα7.2+CD161+ CD8+ T cell (mucosal-associated invariant T cells) subsets in the small intestinal graft as a proportion of total T cells, categorised by time post-transplant (n=41; mean +/- SEM).

(J) The percentage of recipient-derived T cells infiltrating the intestinal graft within unconventional non-Vδ2+ γδ T cell (n=27), Vδ2+ γδ T cell (n=25), and Vα7.2+CD161+ CD8+ T cell subsets (20), categorised by time post-transplant (mean +/- SEM).

(K) Representative flow cytometry plot of CD69 and CD103 expression on donor- and recipient-derived CD8+ and CD4+ T cells in the intestinal graft.

(L) Percentage of donor- and recipient-derived CD8+ and CD4+ T cells in the intestinal graft co-expressing CD69 and CD103 categorised by time post-transplant (n=35; median marked with black line). Blue, CD69-103- cells; Red, CD69+CD103- cells; Black, CD69+CD103+ cells.

For further analysis of surface marker expression, rare populations with fewer than 10 cells were excluded from the analysis (J, L). Statistical analysis performed with 1-way ANOVA with Dunnett's multiple comparisons test. *, $P \leq 0.05$; **, $P \leq 0.01$.

Figure 2. **Transcriptionally distinct tissue resident memory (T_{RM}) T cell populations at single cell level, delineated by CD103 expression.**

(A) Schematic diagram of two scRNAseq experiments. Biopsies of small intestinal transplant tissue were collected from subjects at endoscopy, then dissociated to isolate intestinal lymphocytes. These were sorted by FACS, first with bulk sorting of donor-derived T cells in Experiment 1, then with index sorting of donor-derived CD103- and CD103+ T cells in Experiment 2, before scRNAseq library preparation and sequencing using the 10x Genomics platform (Experiment 1) or the Smart-Seq2 protocol (Experiment 2).

(B) tSNE plot of 974 donor-derived T cells from a single subject showing four transcriptionally distinct populations of conventional CD4+ and CD8+ T cells.

(C) Dot plot of key gene identifiers for the four clusters showing two clusters of CD8+ T cells, and two clusters of CD4+ T cells, including one containing cells expressing *IL2RA* and *FOXP3*, consistent with a regulatory T cell phenotype. Dot size indicates the proportion of cells in which the gene is present. Colour intensity indicates the mean expression level of the gene in cells in that cluster.

(D) Heatmap indicating hierarchical clustering of gene expression of CD8+ donor-derived T cells from population 1 and population 2. Cell labels above indicate cluster: Red, population 1; Blue, population 2. Genes of interest are highlighted.

(E) tSNE plot showing the expression of key genes upregulated in CD8+ population 2 (top row) or upregulated in CD8+ population 1 (bottom row).

(F) Dot plot showing the expression of 13 genes previously associated with tissue residency in human CD69+ T cells (Kumar et al., 2017). Dot size indicates the

691 proportion of cells in which the gene is present. Colour intensity indicates the mean
692 level of expression of the gene in cells in that cluster.
693 (G) Hierarchical clustering and UMAP plot of 196 index-sorted CD103- and CD103+
694 CD8+ donor-derived T cells from two subjects identified three transcriptionally distinct
695 clusters of conventional CD8+ T cells. Cell labels below the dendrogram indicate the
696 plate used for sorting, the subject, and the CD103 expression determined by index
697 sorting. For UMAP plot: circles, CD103- cells by index-sorting; triangles, CD103+ cells
698 by index-sorting; square, unknown CD103 expression by index-sorting.
699 (H) Volcano plot of differential gene expression between cluster 1 and clusters 2 & 3
700 identified in (G), with genes upregulated (right) or down regulated (left) in clusters 2&3
701 compared to cluster 1. $\log_2$(fold change) is plotted against the FDR-adjusted p-value,
702 with horizontal dotted line at FDR=0.05. Differentially expressed genes are marked in
703 blue, with those differentially expressed both Experiments 1 and 2 marked in red.
704 (I) Correlation of $\log_2$(fold change) between populations 1 vs 2 from Experiment 1
705 (10x Genomics, x-axis) and clusters 2&3 vs cluster 1 from Experiment 2 (Smart-Seq2,
706 y-axis). Blue, genes differentially expressed in both experiments; green, genes
707 differentially expressed in Experiment 1 only; yellow, genes differentially expressed in
708 Experiment 2 only; grey, genes not differentially expressed. Genes shown were
709 expressed in both experiments.
710 (J) Venn diagram showing differentially expressed genes upregulated (red) or
711 downregulated (blue) in cluster 1 (CD103-) of Experiment 2 (Smart-Eeq2), or CD8+
712 population 2 of Experiment 1 (10x Genomics). A core gene set of 30 genes that
713 differentiated the two populations in both experiments are listed.

Figure 3. **Localisation and phenotype of CD103- and CD103+ intestinal T_{RM} CD8+ populations.**

(A) Fluorescence microscopy chip cytometry image of small intestinal transplant mucosa from a single subject 3 months post-transplant. The donor was HLA-A3+, and recipient was HLA-A3-. False colour fluorescence imaging for cytokeratin (grey), CD3 (purple), CD8 (red), CD103 (blue), and HLA-A3 (green). Donor-derived CD8+ CD103+ and CD103- cells are indicated by white and yellow arrows respectively.

(B,C) Phenotypic analysis of CD8+ T cell populations in healthy small intestine.

(B) tSNE representation of CD8+ T cell phenotype from spectral flow cytometry concatenated from 5 healthy control subjects, with expression of the following markers superimposed: CD69 and CD103 (first row); CD161, CD7, CD127, β2-integrin, granzyme K, KLRG1, and Ki-67 (second row). The location of cells co-expressing CD69 and CD103 is indicated. Blue, CD69-103- cells; Red, CD69+CD103- cells; Black, CD69+CD103+ cells.

(C) Proportion of positive cells (CD161, KLRG1, Ki-67) or MFI (CD7, CD127, β2-integrin, granzyme K) of CD8+ T cells, categorised by CD69 and CD103 expression, in small intestinal biopsies from healthy control subjects (n=10). Mean percentage or MFI represented by bars. Connecting lines represent populations from the same subject. Blue, CD69-103- cells; Red, CD69+CD103- cells; Black, CD69+CD103+ cells.

(D-J) Phenotypic analysis of recipient-derived CD8+ T cell populations infiltrating the intestinal transplant graft.

(D) The proportion of recipient-derived CD8+ T cells co-expressing CD69 and CD103 in intestinal transplant grafts, categorised by time post-transplant (n=35). Blue, CD69-103- cells; Red, CD69+CD103- cells; Black, CD69+CD103+ cells.

(E-I) Proportion of CD161+ cells (E), Ki-67+ cells (F) or MFI of CD127 (G), granzyme K (H), and β2 integrin (I) of recipient-derived CD8+ T cells, categorised by CD69 and CD103 expression and time post-transplant, in intestinal transplant grafts (n=23). Mean percentage or MFI represented by bars. Black lines connect populations from the same sample. Blue, CD69-103- cells; Red, CD69+CD103- cells; Black, CD69+CD103+ cells.

(J) Representative histogram of β2 integrin surface expression by circulating, intestinal CD69-, intestinal CD69+CD103-, and intestinal CD69+CD103+ CD8+ T cells.

Statistical analysis performed with one-way ANOVA with Tukey's multiple comparisons test. *, $P \leq 0.05$; **, $P \leq 0.01$; ***, $P \leq 0.001$; ****, $P \leq 0.0001$.

Figure 4. **Functional capacity of small intestinal CD8+ T cell populations.**

(A-D) Cytokine production by small intestinal CD8+ T cells.

Representative histograms of expression, and group summaries of proportion of CD8+ T cells expressing TNFα (A), IFNγ (B), CCL4 (C), and IL-2 (D) after 4-hour stimulation with PMA and ionomycin in the presence of brefeldin A and monensin, categorised by CD69 and CD103 expression, in small intestinal biopsies from healthy control subjects (n=10). Blue, CD69-103- cells; Red, CD69+CD103- cells; Black, CD69+CD103+ cells.

(E) Mean proportion of CD8+ T cells expressing 0, 1, 2, 3, or 4 of the cytokines or

760 chemokines TNFα, IFNγ, CCL4, or IL-2, categorised by CD69 and CD103 co-
761 expression, from small intestinal biopsies from healthy control subjects (n=10).
762 (F) Mean percentage (+/- SEM) of CD8+ T cells co-expressing TNFα, IFNγ, CCL4,
763 or IL-2 production after PMA/ionomycin stimulation as described, categorised by CD69
764 and CD103 expression. Blue, CD69-103- cells; Red, CD69+CD103- cells; Black,
765 CD69+CD103+ cells.
766 Statistical analysis performed with one-way ANOVA with Tukey's multiple
767 comparisons test. *, P ≤ 0.05; **, P ≤ 0.01; ***, P ≤ 0.001.
768
769
770 Figure 5. **Phenotype and function of small intestinal CD4+ T cell populations.**
771 (A) MFI (CD161, CD7, CD127, β2-integrin, granzyme K, and KLRG1) or percentage
772 positive (Ki67) of CD4+ T cells, categorised by CD69 and CD103 expression, in small
773 intestinal biopsies from healthy control subjects (n=10). MFI represented by bars.
774 Connecting lines represent populations from the same subject. Blue, CD69-103- cells;
775 Red, CD69+CD103- cells; Black, CD69+CD103+ cells.
776 (B) MFI of β2-integrin of recipient-derived CD4+ T cells, categorised by CD69 and
777 CD103 expression and time post-transplant, in intestinal transplant grafts (n=21). MFI
778 represented by bars. Blue, CD69-103- cells; Red, CD69+CD103- cells; Black,
779 CD69+CD103+ cells.
780 (C-I) Cytokine production by small intestinal CD4+ T cells.
781 Representative histograms of expression, and group summaries of proportion of
782 CD4+ T cells expressing IL-17A (C), TNFα (D), IFNγ (E), IL-2 (F), CCL-4 (G), and IL-10

(H) after 4-hour stimulation with PMA and ionomycin in the presence of brefeldin A and monensin, categorised by CD69 and CD103 expression, in small intestinal biopsies from healthy control subjects (n=10). Blue, CD69-103- cells; Red, CD69+CD103- cells; Black, CD69+CD103+ cells.

(I) Mean proportion of CD4+ T cells expressing 0, 1, 2, 3, 4, 5, or 6 of the cytokines or chemokines IL-17A, TNFα, IFNγ, CCL4, IL-2, or IL-10, categorised by CD69 and CD103 co-expression, from small intestinal biopsies from healthy control subjects (n=10).

Statistical analysis performed with one-way ANOVA with Tukey's multiple comparisons test. *, $P \leq 0.05$; **, $P \leq 0.01$; ***, $P \leq 0.001$.

Supplemental Figure 1.

(A) Illustration demonstrating the principle of HLA allele congenic cell tracking to identify donor- and recipient-derived T cell populations in the transplanted small intestinal graft using fluorophore-conjugated antibodies to Class I HLA haplotypes discordant between donor and recipient.

(B) Representative flow cytometry plot of Class I HLA non-specific staining (0.01-0.12%) from a non-transplant PBMC sample. Gated on Live CD3+ T cells.

(C) Representative flow cytometry gating scheme for identification of T cell subsets.

(D) Representative histogram of CD161 expression of paired donor- and recipient-derived CD8+ intestinal T cells.

(E) Percentage of CD161+ donor- and recipient-derived CD8+ intestinal T cells

806 categorised by time post-transplant (left), or grouped, with paired samples connected by
807 black lines (right) (n=15; mean +/- SEM).
808 Statistical analysis performed with Wilcoxon matched-pairs signed rank test. *, P ≤
809 0.05.
810
811
812 **Supplemental Figure 2:**
813 (A) Quality control parameters and thresholds for 10x Genomics scRNAseq
814 Experiment 1. Number of genes per cell (left), number of unique molecular identifiers
815 (UMIs) per cell (centre), and percentage of mitochondrial reads per cell (right) are
816 displayed. Each dot represents a single cell, with red and blue lines indicating maximum
817 and minimum thresholds, respectively.
818 (B) Dot plot showing expression in Experiment 1 of *ITGB2* and its potential
819 heterodimeric partner, *ITGAL* in Experiment 1. Other potential heterodimeric alpha
820 integrin partners, *ITGAD*, *ITGAM*, and *ITGAX* were not detected. Dot size indicates the
821 proportion of cells in which the gene is present. Colour intensity indicates the mean
822 expression level of the gene.
823 (C) Violin plots showing expression of *ITGB2* and its potential heterodimeric partner
824 *ITGAL* in Experiment 1. Other potential heterodimeric alpha integrin partners, *ITGAD*,
825 *ITGAM*, and *ITGAX* were not detected.
826
827 (D) Dot plot showing expression in Experiment 1 of 11 genes previously negatively
828 associated with tissue residency (downregulated in human CD69+ cells in comparison

to CD69- T cells; (Kumar et al., 2017)). Dot size indicates the proportion of cells in which the gene is present. Colour intensity indicates the mean expression level of the gene. Other genes in the geneset were not detected in the data (*SBK1*, *NPDC1*, *KRT72*, *SOX13*, *KRT73*, *TSPAN18*, *PTGDS*).

(E) Violin plots showing expression in Experiment 1 of 11 genes previously negatively associated with tissue residency (downregulated in human CD69+ cells in comparison to CD69- T cells; (Kumar et al., 2017)).

(F) Violin plots showing expression in Experiment 1 of 13 genes previously associated with tissue residency in human CD69+ T cells (Kumar et al., 2017), demonstrating discordant expression in conventional T cell clusters.

(G-I) Quality control parameters and thresholds for Smart-Seq2 scRNAseq Experiment 2.

(G) Histogram of number of reads per cell and (H) number of genes per cell. Red and blue lines indicate maximum and minimum thresholds, respectively.

(I) Plot showing the percentage of External RNA Controls Consortium (ERCC) spike-ins per cell against the number of genes per cell. Black line indicates upper threshold.

(J) Violin plots showing expression of *ITGB2* and its potential heterodimeric partners *ITGAL* and *ITGAX* in Experiment 2. *ITGAD* and *ITGAM* were not detected in the data.

Supplemental Figure 3.

(A) Representative expression of CD161, CD7, CD127 (IL7R), ITGB2, and Granzyme K on CD103- (red) and CD103+ (black) donor-derived T cells from the intestinal transplant graft.

(B) The proportion of CD8+ T cells co-expressing CD69 and CD103 in small intestinal biopsies from the duodenum (duo) or ileum from healthy control subjects (n=5 for both duodenum and ileum). Blue, CD69-103- cells; Red, CD69+CD103- cells; Black, CD69+CD103+ cells.

(C) Representative flow cytometry gating of CD4+ CD25+CD127lo T cells. Percentage of donor- or recipient-derived intestinal CD4+ CD25+CD127lo T cells. Connecting lines represent populations from the same subject (n=23).

References

Adachi, T., T. Kobayashi, E. Sugihara, T. Yamada, K. Ikuta, S. Pittaluga, H. Saya, M. Amagai, and K. Nagao. 2019. Hair follicle-derived IL-7 and IL-15 mediate skin-resident memory T cell homeostasis and lymphoma. *Nature Medicine*. 1–10. doi:10.1038/nm.3962.

Andrews, T.S., Andrews, T.S., and M. Hemberg. 2018. M3Drop: dropout-based feature selection for scRNASeq. *Bioinformatics*. 35:2865–2867. doi:10.1093/bioinformatics/bty1044.

Ariotti, S., M.A. Hogenbirk, F.E. Dijkgraaf, L.L. Visser, M.E. Hoekstra, J.-Y. Song, H. Jacobs, J.B. Haanen, and T.N. Schumacher. 2014. T cell memory. Skin-resident memory CD8$^+$ T cells trigger a state of tissue-wide pathogen alert. *Science*. 346:101–105. doi:10.1126/science.1254803.

Bartolomé-Casado, R., O.J.B. Landsverk, S.K. Chauhan, L. Richter, D. Phung, V. Greiff, L.F. Risnes, Y. Yao, R.S. Neumann, S. Yaqub, O. Øyen, R. Horneland, E.M. Aandahl, V. Paulsen, L.M. Sollid, S.-W. Qiao, E.S. Bækkevold, and F.L. Jahnsen. 2019. Resident memory CD8 T cells persist for years in human small intestine. *J Exp Med*. 157:jem.20190414–23. doi:10.1084/jem.20190414.

Bergsbaken, T., and M.J. Bevan. 2015. Proinflammatory microenvironments within the intestine regulate the differentiation of tissue-resident CD8+ T cells responding to infection. *Nat Immunol*. 16:406–414. doi:10.1038/ni.3108.

883 Beura, L.K., S. Wijeyesinghe, E.A. Thompson, M.G. Macchietto, P.C. Rosato, M.J.
884 Pierson, J.M. Schenkel, J.S. Mitchell, V. Vezys, B.T. Fife, S. Shen, and D.
885 Masopust. 2018. T Cells in Nonlymphoid Tissues Give Rise to Lymph- Node-
886 Resident Memory T Cells. *Immunity*. 48:327–338.e5.
887 doi:10.1016/j.immuni.2018.01.015.

888 Bolger, A.M., M. Lohse, and B. Usadel. 2014. Trimmomatic: a flexible trimmer for
889 Illumina sequence data. *Bioinformatics*. 30:2114–2120.
890 doi:10.1093/bioinformatics/btu170.

891 Boutet, M., L. Gauthier, M. Leclerc, G. Gros, V. de Montpreville, N. Théret, E.
892 Donnadieu, and F. Mami-Chouaib. 2016. TGFβ Signaling Intersects with CD103
893 Integrin Signaling to Promote T-Lymphocyte Accumulation and Antitumor Activity in
894 the Lung Tumor Microenvironment. *Cancer Res*. 76:1757–1769. doi:10.1158/0008-
895 5472.CAN-15-1545.

896 Butler, A., P. Hoffman, P. Smibert, E. Papalexi, and R. Satija. 2018. Integrating single-
897 cell transcriptomic data across different conditions, technologies, and species. *Nat*
898 *Biotechnol*. 36:411–420. doi:10.1038/nbt.4096.

899 de Leur, K., M. Dieterich, D.A. Hesselink, O.B.J. Corneth, F.J.M.F. Dor, G.N. Graav,
900 A.M.A. Peeters, A. Mulder, H.J.A.N. Kimenai, F.H.J. Claas, M.C.C.-V. Groningen,
901 L.J.W. Laan, R.W. Hendriks, and C.C. Baan. 2019. Characterization of donor and
902 recipient CD8+ tissue-resident memory T cells in transplant nephrectomies. *Sci*
903 *Rep*. 1–12. doi:10.1038/s41598-019-42401-9.

904 Dobin, A., C.A. Davis, F. Schlesinger, J. Drenkow, C. Zaleski, S. Jha, P. Batut, M.
905 Chaisson, and T.R. Gingeras. 2012. STAR: ultrafast universal RNA-seq aligner.
906 *Bioinformatics*. 29:15–21. doi:10.1093/bioinformatics/bts635.

907 Fagerholm, S.C., C. Guenther, M. Llort Asens, T. Savinko, and L.M. Uotila. 2019.
908 Beta2-Integrins and Interacting Proteins in Leukocyte Trafficking, Immune
909 Suppression, and Immunodeficiency Disease. *Front. Immunol.* 10:549–10.
910 doi:10.3389/fimmu.2019.00254.

911 Feau, S., R. Arens, S. Togher, and S.P. Schoenberger. 2011. Autocrine IL-2 is required
912 for secondary population expansion of CD8+ memory T cells. *Nat Immunol*. 12:908–
913 913. doi:10.1038/ni.2079.

914 Fergusson, J.R., M.H.H.U. hn, L. Swadling, L.J. Walker, A. Kurioka, A. Llibre, A.
915 Bertoletti, G.H.A. nder, E.W. Newell, M.M. Davis, E.S.-E.O. m, F. Powrie, S.
916 Capone, A. Folgori, E. Barnes, C.B. Willberg, J.E. Ussher, and P. Klenerman. 2015.
917 CD161intCD8+ T cells: a novel population of highly functional, memory CD8+ T
918 cells enriched within the gut. 1–13. doi:10.1038/mi.2015.69.

919 Fu, J., J. Zuber, M. Martinez, B. Shonts, A. Obradovic, H. Wang, S.-P. Lau, A. Xia, E.E.
920 Waffarn, K. Frangaj, T.M. Savage, M.T. Simpson, S. Yang, X.V. Guo, M. Miron, T.
921 Senda, K. Rogers, A. Rahman, S.-H. Ho, Y. Shen, A. Griesemer, D.L. Farber, T.

922 Kato, and M. Sykes. 2019. Human Intestinal Allografts Contain Functional
923 Hematopoietic Stem and Progenitor Cells that Are Maintained by a Circulating Pool.
924 *Stem Cell*. 24:227–239.e8. doi:10.1016/j.stem.2018.11.007.

925 Gebhardt, T., P.G. Whitney, A. Zaid, L.K. Mackay, A.G. Brooks, W.R. Heath, F.R.
926 Carbone, and S.N. Mueller. 2011. Different patterns of peripheral migration by
927 memory CD4+ and CD8+ T cells. *Nature*. 477:216–219. doi:10.1038/nature10339.

928 Gutierrez-Arcelus, M., N. Teslovich, A.R. Mola, R.B. Polidoro, A. Nathan, H. Kim, S.
929 Hannes, K. Slowikowski, G.F.M. Watts, I. Korsunsky, M.B. Brenner, S.
930 Raychaudhuri, and P.J. Brennan. 2019. Lymphocyte innateness defined by
931 transcriptional states reflects a balance between proliferation and effector functions.
932 *Nature Communications*. 1–15. doi:10.1038/s41467-019-08604-4.

933 Harris, R.A., D. Nagy-Szakal, S.A. Mir, E. Frank, R. Szigeti, J.L. Kaplan, J. Bronsky, A.
934 Opekun, G.D. Ferry, H. Winter, and R. Kellermayer. 2014. DNA methylation-
935 associated colonic mucosal immune and defense responses in treatment-naïve
936 pediatric ulcerative colitis. *Epigenetics*. 9:1131–1137. doi:10.4161/epi.29446.

937 Hennig, C., N. Adams, and G. Hansen. 2009. A versatile platform for comprehensive
938 chip-based explorative cytometry. *Cytometry*. 75A:362–370.
939 doi:10.1002/cyto.a.20668.

940 Hombrink, P., C. Helbig, R.A. Backer, B. Piet, A.E. Oja, R. Stark, G. Brasser, A.
941 Jongejan, R.E. Jonkers, B. Nota, O. Basak, H.C. Clevers, P.D. Moerland, D. Amsen,
942 and R.A.W. van Lier. 2016. Programs for the persistence, vigilance and control of
943 human CD8+ lung-resident memory T cells. *Nat Immunol*. 17:1467–1478.
944 doi:10.1038/ni.3589.

945 Kennedy, N.A., A.T. Adams, R. Kalla, S. Heath, K.R.O.A. Leary, H. Drummond, D.C.
946 Wilson, I.G. Gut, E.R. Nimmo, J. Satsangi, G. Lauc, H. Campbell, D.P.B. McGovern,
947 V. Annese, V.Z. scaron, I.K. Permberton, M. Wuhrer, D. Kolarich, D.L. Fernandes,
948 E. Theorodorou, V. Merrick, D.I. Spencer, R.A. Gardner, R. Doran, A. Shubhakar, R.
949 Boyapati, I. Rudan, P. Lionetti, I.T.C.A.C.I. cacute, J.K.S.T. cacute, F.V.C.K. cacute,
950 J.S. tambuk, M. Novokmet, M.P.C.I.C.B. cacute, O. Gornik, A. Andriulli, L. Cantoro,
951 G. Sturniolo, G. Fiorino, N. Manetti, A. Latiano, A. Kohn, R.D.R.I. agrave, S.
952 Danese, I.D. Arnott, C.L. Noble, C.W. Lees, A.G. Shand, G.-T. Ho, M.G. Dunlop, L.
953 Murphy, J. Gibson, L. Evenden, N. Wrobel, T. Gilchrist, A. Fawkes, G.S.M.
954 Kammeijer, F. Clerc, N. de Haan, A. Vojta, I.S.Z. ija, D. Markulin, M.K. cacute, P.D.
955 cacute, Y. Aulchenko, T. van den Heuve, D. Jonkers, M. Pierik, S. Vatn, P. Ricanek,
956 J.O.R. Jahnsen, P. You, J.S.O. Ivernes, A.B. Frengen, T.M.T.A. s, A.E.F. Moen,
957 F.A. Dahl, J.C.L.O. m, G.S. Ekeland, T.E. Detlie, A.S.V. Keita, J.D.S.O. derholm, H.
958 Hjortswang, J. Halfvarson, D. Bergemalm, F.G.O. n, M.D.A. Amato, L.T.O. rkvist, F.
959 Hjelm, M. Gullberg, N. Nordberg, A. Ocklind, E. Pettersson, D. Ekman, M. Sundell,
960 E. Modig, A.C.E.M. Veillard, R. Schoemans, et al. 2016. Integrative epigenome-wide
961 analysis demonstrates that DNA methylation may mediate genetic risk in
962 inflammatory bowel disease. *Nature Communications*. 7:1–14.

963 doi:10.1038/ncomms13507.

964 Kiselev, V.Y., K. Kirschner, M.T. Schaub, T. Andrews, A. Yiu, T. Chandra, K.N.
965 Natarajan, W. Reik, M. Barahona, A.R. Green, and M. Hemberg. 2017. SC3:
966 consensus clustering of single-cell RNA-seq data. *Nat Meth*. 14:483–486.
967 doi:10.1038/nmeth.4236.

968 Konnikova, L., G. Boschetti, A. Rahman, V. Mitsialis, J. Lord, C. Richmond, V.T. Tomov,
969 W. Gordon, S. Jelinsky, J. Canavan, A. Liss, S. Wall, M. Field, F. Zhou, J.D.
970 Goldsmith, M. Bewtra, D.T. Breault, M. Merad, and S.B. Snapper. 2018. High-
971 dimensional immune phenotyping and transcriptional analyses reveal robust
972 recovery of viable human immune and epithelial cells from frozen gastrointestinal
973 tissue. *Mucosal Immunology*. 1–10. doi:10.1038/s41385-018-0047-y.

974 Kumar, B.V., W. Ma, M. Miron, T. Granot, R.S. Guyer, D.J. Carpenter, T. Senda, X.
975 Sun, S.-H. Ho, H. Lerner, A.L. Friedman, Y. Shen, and D.L. Farber. 2017. Human
976 Tissue-Resident Memory T Cells Are Defined by Core Transcriptional and
977 Functional Signatures in Lymphoid and Mucosal Sites. *CellReports*. 20:2921–2934.
978 doi:10.1016/j.celrep.2017.08.078.

979 Leng, T., H.D. Akther, C.-P. Hackstein, K. Powell, T. King, M. Friedrich, Z.
980 Christoforidou, S. McCuaig, M. Neyazi, C.V. Arancibia-Cárcamo, J. Hagel, F.
981 Powrie, R.S. Peres, V. Millar, D. Ebner, R. Lamichhane, J. Ussher, T.S.C. Hinks, E.
982 Marchi, C. Willberg, P. Klenerman, and O.I. Investigators3. 2019. TCR and
983 Inflammatory Signals Tune Human MAIT Cells to Exert Specific Tissue Repair and
984 Effector Functions. *CellReports*. 28:3077–3091.e5.
985 doi:10.1016/j.celrep.2019.08.050.

986 Li, H., Li, H., B. Handsaker, B. Handsaker, A. Wysoker, A. Wysoker, T. Fennell, T.
987 Fennell, J. Ruan, J. Ruan, N. Homer, N. Homer, G. Marth, G. Marth, G. Abecasis,
988 G. Abecasis, R. Durbin, R. Durbin, and 1000 Genome Project Data Processing
989 Subgroup. 2009. The Sequence Alignment/Map format and SAMtools.
990 *Bioinformatics*. 25:2078–2079. doi:10.1093/bioinformatics/btp352.

991 Liao, Y., Liao, Y., G.K. Smyth, G.K. Smyth, W. Shi, and W. Shi. 2014. featureCounts: an
992 efficient general purpose program for assigning sequence reads to genomic
993 features. *Bioinformatics*. 30:923–930. doi:10.1093/bioinformatics/btt656.

994 Liu, D., Y.T. Bryceson, T. Meckel, G. Vasiliver-Shamis, M.L. Dustin, and E.O. Long.
995 2009. Integrin-Dependent Organization and Bidirectional Vesicular Traffic at
996 Cytotoxic Immune Synapses. *Immunity*. 31:99–109.
997 doi:10.1016/j.immuni.2009.05.009.

998 Lun, A.T.L., D.J. McCarthy, and J.C. Marioni. 2016. A step-by-step workflow for low-
999 level analysis of single-cell RNA-seq data with Bioconductor. *F1000Res*. 5:2122.
1000 doi:10.12688/f1000research.9501.2.

1001 Mackay, L.K., and A. Kallies. 2017. Transcriptional Regulation of Tissue-Resident

1002 Lymphocytes. *Trends in Immunology*. 38:94–103. doi:10.1016/j.it.2016.11.004.

1003 Mackay, L.K., M. Minnich, N.A.M. Kragten, Y. Liao, B. Nota, C. Seillet, A. Zaid, K. Man,
1004 S. Preston, D. Freestone, A. Braun, E. Wynne-Jones, F.M. Behr, R. Stark, D.G.
1005 Pellicci, D.I. Godfrey, G.T. Belz, M. Pellegrini, T. Gebhardt, M. Busslinger, W. Shi,
1006 F.R. Carbone, R.A.W. van Lier, A. Kallies, and K.P.J.M. van Gisbergen. 2016. Hobit
1007 and Blimp1 instruct a universal transcriptional program of tissue residency in
1008 lymphocytes. *Science*. 352:459–459. doi:10.1126/science.aad2035.

1009 Mayassi, T., K. Ladell, H. Gudjonson, J.E. McLaren, D.G. Shaw, M.T. Tran, J.J.
1010 Rokicka, I. Lawrence, J.-C. Grenier, V. van Unen, C. Ciszewski, M. Dimaano, H.E.
1011 Sayegh, V. Kumar, C. Wijmenga, P.H.R. Green, R. Gokhale, H. Jericho, C.E.
1012 Semrad, S. Guandalini, A.R. Dinner, S.S. Kupfer, H.H. Reid, L.B. Barreiro, J.
1013 Rossjohn, D.A. Price, and B. Jabri. 2019. Chronic Inflammation Permanently
1014 Reshapes Tissue-Resident Immunity in Celiac Disease. *Cell*. 1–35.
1015 doi:10.1016/j.cell.2018.12.039.

1016 McCarthy, D.J., K.R. Campbell, A.T.L. Lun, and Q.F. Wills. 2017. Scater: pre-
1017 processing, quality control, normalization and visualization of single-cell RNA-seq
1018 data in R. *Bioinformatics*. 247:btw777–1186. doi:10.1093/bioinformatics/btw777.

1019 McInnes, L., J. Healy, and J. Melville. 2018. UMAP: Uniform Manifold Approximation
1020 and Projection for Dimension Reduction. arXiv preprint arXiv:1802.03426

1021 McNamara, H.A., Y. Cai, M.V. Wagle, Y. Sontani, C.M. Roots, L.A. Miosge, J.H.
1022 O'Connor, H.J. Sutton, V.V. Ganusov, W.R. Heath, P. Bertolino, C.G. Goodnow, I.A.
1023 Parish, A. Enders, and I.A. Cockburn. 2017. Up-regulation of LFA-1 allows liver-
1024 resident memory T cells to patrol and remain in the hepatic sinusoids. *Science*
1025 *Immunology*. 2:1–11. doi:10.1126/sciimmunol.aaj1996.

1026 Miao, Z., K. Deng, X. Wang, and X. Zhang. 2018. DEsingle for detecting three types of
1027 differential expression in single-cell RNA-seq data. *Bioinformatics*. 34:3223–3224.
1028 doi:10.1093/bioinformatics/bty332.

1029 Oja, A.E., B. Piet, C. Helbig, R. Stark, D. van der Zwan, H. Blaauwgeers, E.B.M.
1030 Remmerswaal, D. Amsen, R.E. Jonkers, P.D. Moerland, M.A. Nolte, R.A.W. van
1031 Lier, and P. Hombrink. 2017. Trigger-happy resident memory CD4+ T cells inhabit
1032 the human lungs. *Mucosal Immunology*. 11:654–667. doi:10.1038/mi.2017.94.

1033 Pallett, L.J., J. Davies, E.J. Colbeck, F. Robertson, N. Hansi, N.J.W. Easom, A.R.
1034 Burton, K.A. Stegmann, A. Schurich, L. Swadling, U.S. Gill, V. Male, T. Luong, A.
1035 Gander, B.R. Davidson, P.T.F. Kennedy, and M.K. Maini. 2017. IL-2high tissue-
1036 resident T cells in the human liver: Sentinels for hepatotropic infection. *J Exp Med*.
1037 214:1567–1580. doi:10.1084/jem.20162115.

1038 Park, S.L., T. Gebhardt, and L.K. Mackay. 2019. Tissue-Resident Memory T Cells in
1039 Cancer Immunosurveillance. *Trends in Immunology*. 1–13.
1040 doi:10.1016/j.it.2019.06.002.

1041 Picelli, S., Å.K. Björklund, O.R. Faridani, S. Sagasser, G. Winberg, and R. Sandberg.
1042 2013. Smart-seq2 for sensitive full-length transcriptome profiling in single cells. *Nat*
1043 *Meth*. 10:1096–1098. doi:10.1038/nmeth.2639.

1044 Picelli, S., O.R. Faridani, A.S.K.B.O. rklund, G.O.S. Winberg, S. Sagasser, and R.
1045 Sandberg. 2014. Full-length RNA-seq from single cells using Smart-seq2. *Nat*
1046 *Protoc*. 9:171–181. doi:10.1038/nprot.2014.006.

1047 Provine, N.M., B. Binder, M.E.B. FitzPatrick, A. Schuch, L.C. Garner, K.D. Williamson,
1048 B. van Wilgenburg, R. Thimme, P. Klenerman, and M. Hofmann. 2018. Unique and
1049 Common Features of Innate-Like Human Vδ2+ γδT Cells and Mucosal-Associated
1050 Invariant T Cells. *Front. Immunol.* 9:120–12. doi:10.3389/fimmu.2018.00756.

1051 Raeber, M.E., Y. Zurbuchen, D. Impellizzieri, and O. Boyman. 2018. The role of
1052 cytokines in T-cell memory in health and disease. *Immunol Rev*. 283:176–193.
1053 doi:10.1111/imr.12644.

1054 Román, J., N. Planell, J.J. Lozano, M. Aceituno, M. Esteller, C. Pontes, D. Balsa, M.
1055 Merlos, J. Panés, and A. Salas. 2013. Evaluation of Responsive Gene Expression
1056 as a Sensitive and Specific Biomarker in Patients with Ulcerative Colitis. *Inflamm*
1057 *Bowel Dis*. 19:221–229. doi:10.1002/ibd.23020.

1058 Sancho, D., M. Gómez, and F. Sánchez-Madrid. 2005. CD69 is an immunoregulatory
1059 molecule induced following activation. *Trends in Immunology*. 26:136–140.
1060 doi:10.1016/j.it.2004.12.006.

1061 Schenkel, J.M., K.A. Fraser, L.K. Beura, K.E. Pauken, V. Vezys, and D. Masopust.
1062 2014. Resident memory CD8 T cells trigger protective innate and adaptive immune
1063 responses. *Science*. 346:98–101. doi:10.1126/science.1254536.

1064 Shiow, L.R., D.B. Rosen, N. Brdičková, Y. Xu, J. An, L.L. Lanier, J.G. Cyster, and M.
1065 Matloubian. 2006. CD69 acts downstream of interferon-α/β to inhibit S1P1 and
1066 lymphocyte egress from lymphoid organs. *Nature*. 440:540–544.
1067 doi:10.1038/nature04606.

1068 Snyder, M.E., M.O. Finlayson, T.J. Connors, P. Dogra, T. Senda, E. Bush, D.
1069 Carpenter, C. Marboe, L. Benvenuto, L. Shah, H. Robbins, J.L. Hook, M. Sykes, F.
1070 D'Ovidio, M. Bacchetta, J.R. Sonett, D.J. Lederer, S. Arcasoy, P.A. Sims, and D.L.
1071 Farber. 2019. Generation and persistence of human tissue-resident memory T cells
1072 in lung transplantation. *Science Immunology*. 4:1–17.

1073 Stuart, T., A. Butler, P. Hoffman, C. Hafemeister, E. Papalexi, W.M. Mauck, W.M.
1074 Mauck III, Y. Hao, M. Stoeckius, P. Smibert, and R. Satija. 2019. Comprehensive
1075 Integration of Single-Cell Data. *Cell*. 177:1888–1902.e21.
1076 doi:10.1016/j.cell.2019.05.031.

1077 Szabo, P.A., M. Miron, and D.L. Farber. 2019. Location, location, location: Tissue
1078 resident memory T cells in mice and humans. *Science Immunology*. 4:1–12.

1079 doi:10.1126/sciimmunol.aas9673.

1080 Thome, J.J.C., N. Yudanin, Y. Ohmura, M. Kubota, B. Grinshpun, T. Sathaliyawala, T.
1081 Kato, H. Lerner, Y. Shen, and D.L. Farber. 2014. Spatial Map of Human T Cell
1082 Compartmentalization and Maintenance over Decades of Life. *Cell*. 159:814–828.
1083 doi:10.1016/j.cell.2014.10.026.

1084 Verma, N.K., E. Dempsey, A. Long, A. Davies, S.P. Barry, P.G. Fallon, Y. Volkov, and
1085 D. Kelleher. 2012. Leukocyte Function-associated Antigen-1/Intercellular Adhesion
1086 Molecule-1 Interaction Induces a Novel Genetic Signature Resulting in T-cells
1087 Refractory to Transforming Growth Factor-β Signaling. *Journal of Biological*
1088 *Chemistry*. 287:27204–27216. doi:10.1074/jbc.M112.376616.

1089 Walsh, D.A., H. Borges da Silva, L.K. Beura, C. Peng, S.E. Hamilton, D. Masopust, and
1090 S.C. Jameson. 2019. The Functional Requirement for CD69 in Establishment of
1091 Resident Memory CD8 +T Cells Varies with Tissue Location. *J.I.* 203:946–955.
1092 doi:10.4049/jimmunol.1900052.

1093 Zimmerli, S.C., A. Harari, C. Cellerai, F. Vallelian, P.-A. Bart, and G. Pantaleo. 2005.
1094 HIV-1-specific IFN-γ/IL-2-secreting CD8 T cells support CD4-independent
1095 proliferation of HIV-1-specific CD8 T cells. *Proc. Natl. Acad. Sci. U.S.A.* 102:7239–6.
1096 doi:10.1073/pnas.0502393102.

1097 Zuber, J., B. Shonts, S.P. Lau, A. Obradovic, J. Fu, S. Yang, M. Lambert, S. Coley, J.
1098 Weiner, J. Thome, S. DeWolf, D.L. Farber, Y. Shen, S. Caillat-Zucman, G. Bhagat,
1099 A. Griesemer, M. Martinez, T. Kato, and M. Sykes. 2016. Bidirectional intragraft
1100 alloreactivity drives the repopulation of human intestinal allografts and correlates
1101 with clinical outcome. *Science Immunology*. 1:eaah3732–eaah3732.
1102 doi:10.1126/sciimmunol.aah3732.

1103 Zuber, J., S. Rosen, B. Shonts, B. Sprangers, T.M. Savage, S. Richman, S. Yang, S.P.
1104 Lau, S. DeWolf, D. Farber, G. Vlad, E. Zorn, W. Wong, J. Emond, B. Levin, M.
1105 Martinez, T. Kato, and M. Sykes. 2015. Macrochimerism in Intestinal
1106 Transplantation: Association With Lower Rejection Rates and Multivisceral
1107 Transplants, Without GVHD. *American Journal of Transplantation*. 15:2691–2703.
1108 doi:10.1111/ajt.13325.

1109 Zundler, S., E. Becker, M. Spocinska, M. Slawik, L. Parga-Vidal, R. Stark, M. Wiendl, R.
1110 Atreya, T. Rath, M. Leppkes, K. Hildner, R.X.O.L.X. pez-Posadas, S.X.R. Lukassen,
1111 A.B. Ekici, C. Neufert, I. Atreya, K.P.J.M. Gisbergen, and M.F. Neurath. 2019. Hobit-
1112 and Blimp-1-driven CD4+ tissue-resident memory T cells control chronic intestinal
1113 inflammation. *Nature Immunology. 20:*288-300. doi:10.1038/s41590-018-0298-5.

1114

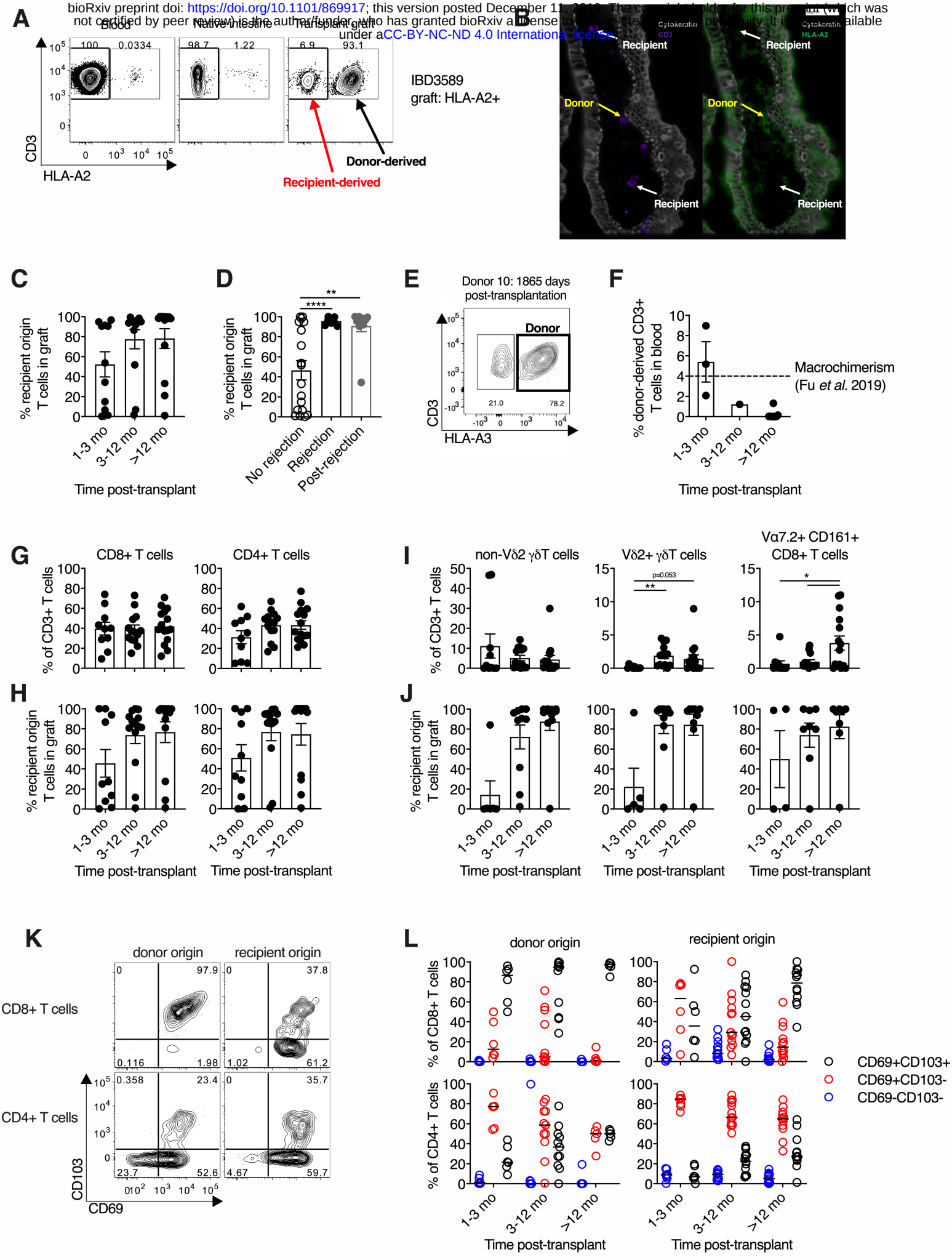

Figure 1

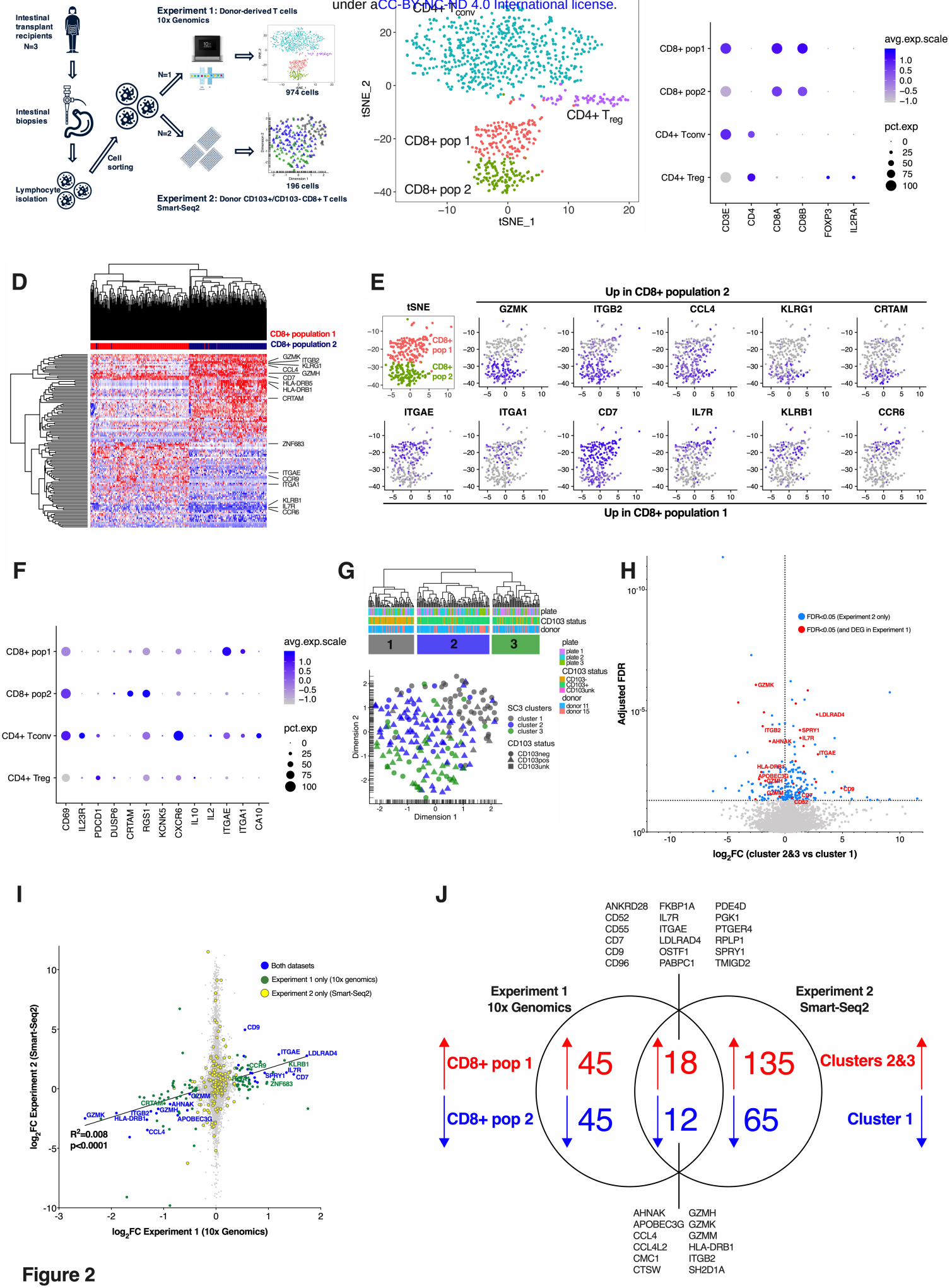

Figure 2

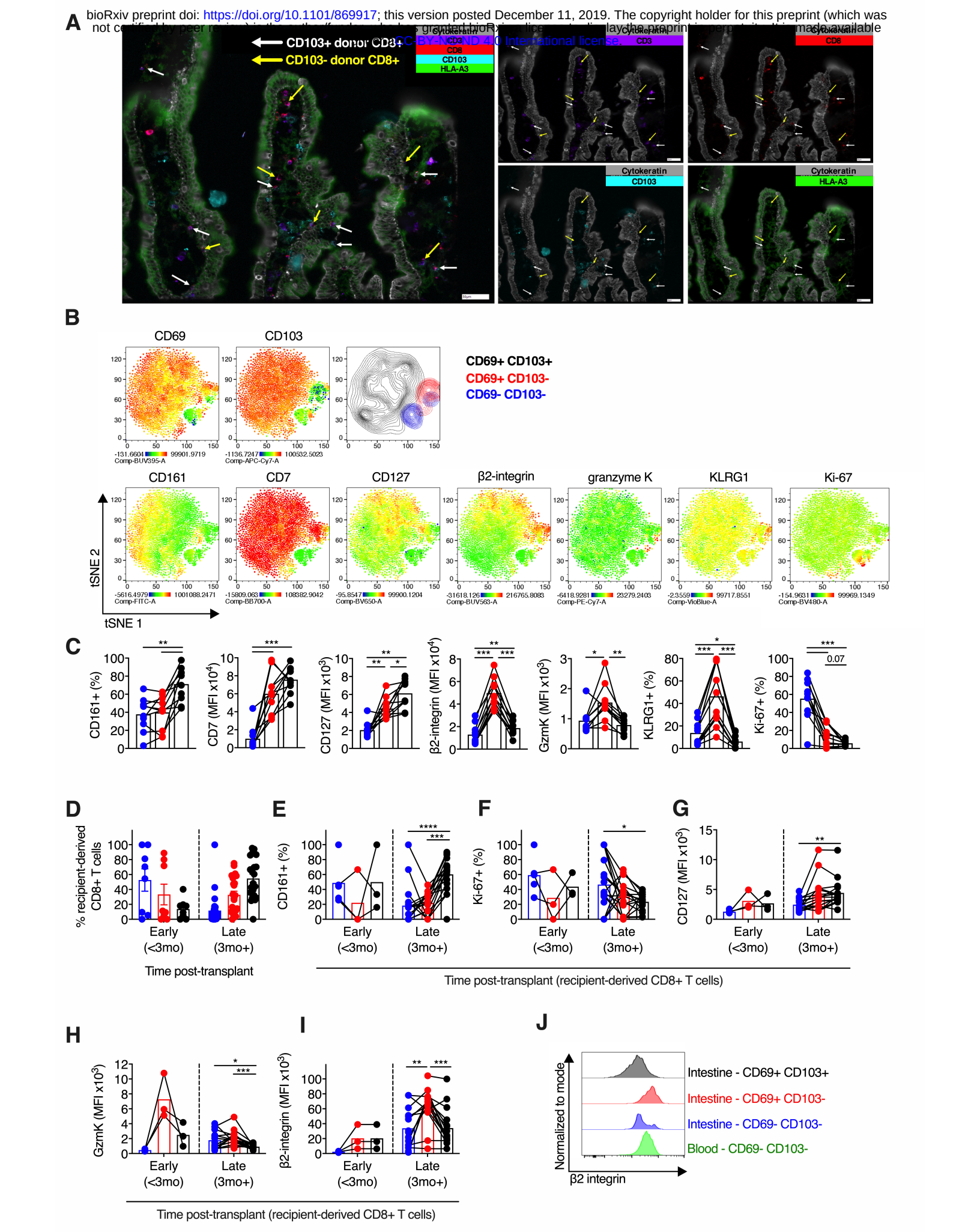

Figure 3

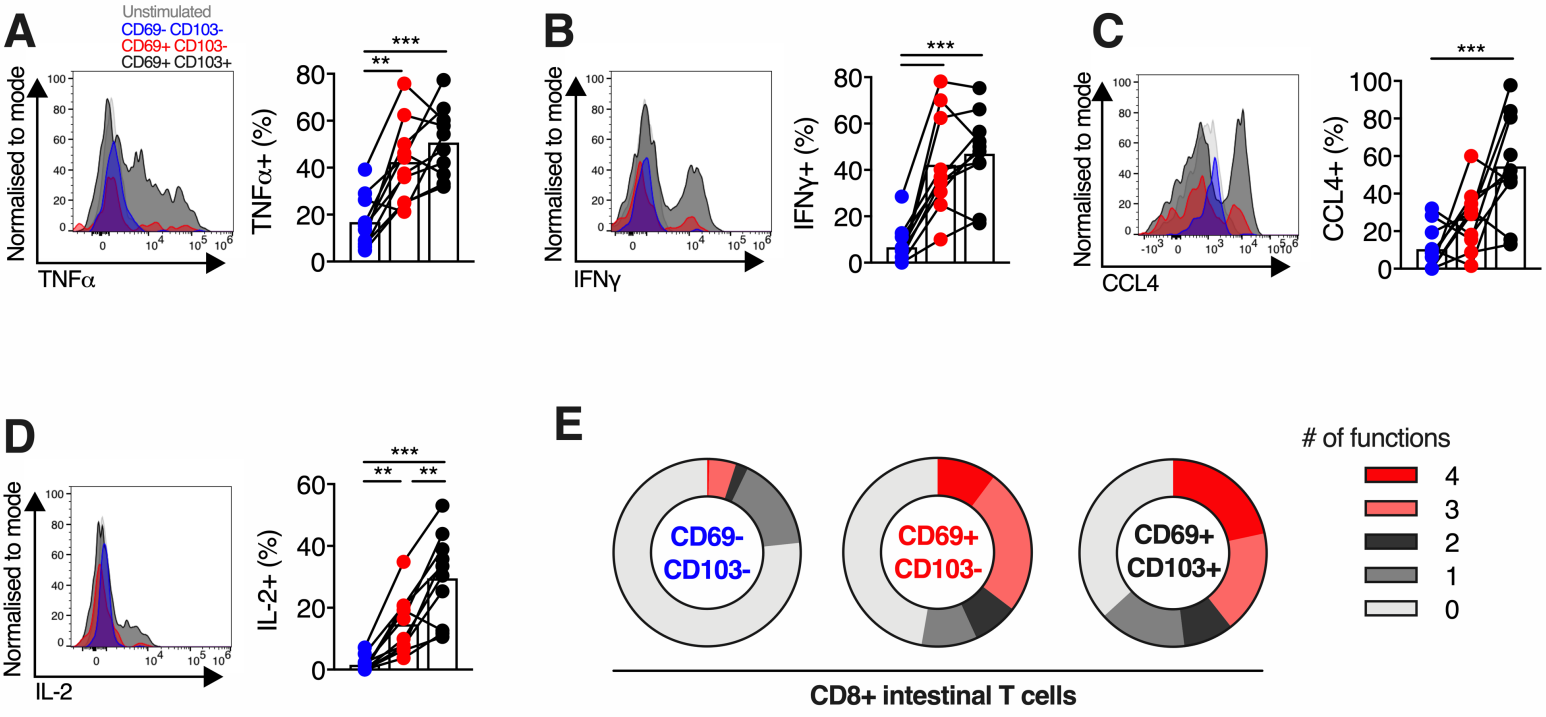

Figure 4

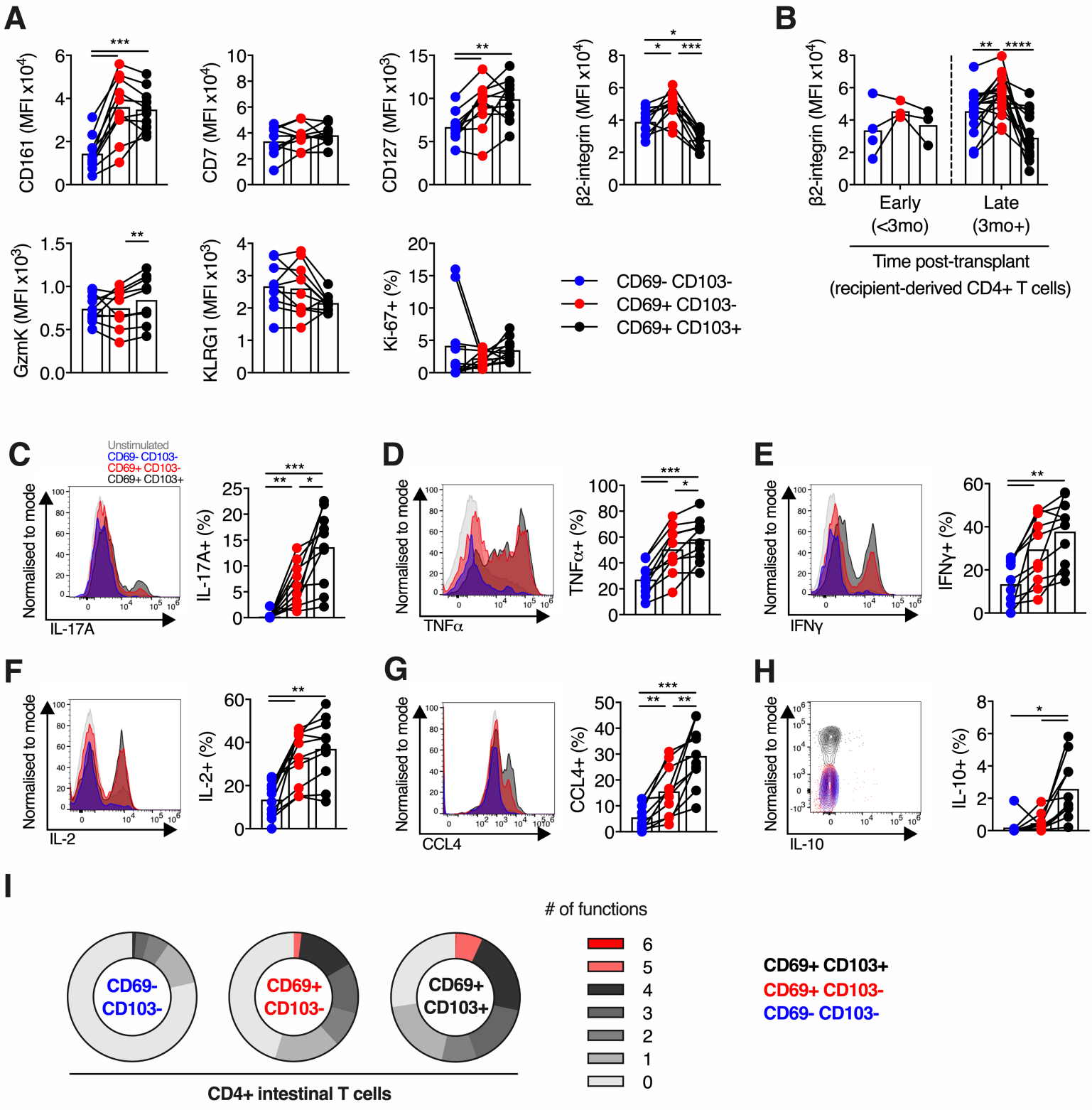

Figure 5